Grating-coupler-induced intersubband resonances in electron inversion layers of silicon

D. Heitmann and U. Mackens
Institut für Angewandte Physik, Universität Hamburg, Jungiusstrasse 11, D-2000 Hamburg 36, West Germany
(Received 17 May 1985)

Resonant intersubband transitions in electron inversion layers on the three principal surfaces of Si have been studied with efficient grating couplers. For Si(111) and Si(110) both directly parallel excited and grating-coupler-induced depolarization-shifted resonances are observed and their dependence on the surface electric and depletion fields studied. For Si(100) intersubband resonances are investigated up to charge densities $N_s = 1.2 \times 10^{13}$ cm^{-2}. At high densities transitions in the primed subband system are observed. Also for Si(100), there is evidence for parallel excited resonance transitions, which are strictly forbidden for vertical transitions ($\Delta k = 0$), but become allowed for grating-coupler-induced nonvertical transitions ($\Delta k \neq 0$). On all three surfaces a strong interaction of the intersubband resonances with optical phonons in the adjacent SiO_2 layer is found.

I. INTRODUCTION

In metal-oxide-semiconductor (MOS) structures of silicon, electrons can be confined in a very narrow potential well at the Si-SiO_2 interface. The one-particle energy spectrum of the electrons,

$$E_i(k_x,k_y) = E_i + \frac{\hbar^2 k_x^2}{2m_x} + \frac{\hbar^2 k_y^2}{2m_y} ,$$

consists of a set of subbands (index i) that arises from the quantized motion perpendicular to the surface (z direction) and the continuous dispersion parallel to the surface (x-y plane).[1] A powerful tool for the investigation of the subband structure is the excitation of resonant intersubband transitions with far-infrared (FIR) radiation (e.g., Refs. 2 and 3).

The excitation of intersubband resonances characterizes the oscillatory motion of the electrons normal to the interface. Thus on the highly symmetric Si(100) surface a perpendicular component E_z of the exciting FIR field is necessary to induce intersubband resonances.[3] For Si(110) and Si(111) excitation is also possible with parallel field components[4,5] due to the tilted ellipsoidal energy contours[6] which couple the components of the surface current j_z with the parallel components j_x and j_y.

Investigation of intersubband resonances on Si(110) and Si(111) has become of recent interest both experimentally[7-10] and theoretically.[5,11] One of the points of interest there is that the resonance energies differ from the subband separation due to exciton and depolarization effects, of which the latter acts differently for parallel and perpendicular excitations.[4,5,7-9]

Excitation with perpendicular polarization needs special experimental arrangements to induce a z component of the FIR field, E_z. Transmission lines[3] and prism arrangements[12] have been used. This has limited experimental investigations of perpendicularly excited intersubband resonances on Si so far to resonance energies below 250 cm^{-1} with correspondingly low electron densities ($N_s < 2 \times 10^{12}$ cm^{-2}).

A different technique to excite intersubband resonances uses grating couplers.[13,14] In this case the gate of the MOS sample consists of periodic metal stripes of low and high conductivity (see Fig. 1). Normally, incident FIR radiation induces in the near field of the grating z components of the electric field, E_z, which make perpendicular excitation of intersubband resonances possible. The grating-coupler-induced x and z components of the incident radiation are spatially modulated with a periodicity a. Thus the grating coupler induces nonvertical transitions ($\Delta k = 2\pi n/a$, $n = \pm 1, \pm 2, \ldots$). These nonvertical transitions have some interesting properties which are observed in our experiments here and will be discussed below. Grating-coupler-induced intersubband resonances have recently been treated theoretically, too.[15,16]

In the following we will report on extensive experimental studies of grating-coupler-induced intersubband resonances on two-dimensional (2D) electron space-charge layers at the three principal surfaces of Si. Efficient grating couplers and rapid-scan Fourier-transform spectroscopy make it possible to investigate perpendicularly excited intersubband resonances up to charge densities of 1.2×10^{13} cm^{-2}.

For Si(100) three transitions from the ground-state subband E_0, $0 \rightarrow 1$, $0 \rightarrow 2$, $0 \rightarrow 3$, are observed. At high charge densities transitions $0' \rightarrow 1'$ in a second subband system[1] are studied. In substrate-bias experiments a strong influence of the depletion field is investigated.

For Si(111) and Si(110) the spectra contain resonant transitions from both directly induced parallel excitation and grating-coupler-induced perpendicular excitation. Here we can study the strength of the depolarization shift in its dependence on the charge density N_s, the depletion field F_{depl}, and for different transitions ($0 \rightarrow 1$, $0 \rightarrow 2$).

A unique feature of grating-coupler-induced intersubband resonances is that for Si(100) excitation of nondepolarization-shifted transitions is possible. Parallel excited vertical transitions are strictly forbidden for the symmetry of Si(100), but they become allowed for the grating-coupler-induced nonvertical transitions.

Also characteristic for our grating-coupler experiments

is that they induce a strong interaction of intersubband excitation with optical phonons in the adjacent SiO_2 layer.

II. THEORETICAL REMARKS

A. Subband structure and intersubband resonances

The potential well at the SiO_2-Si interface of a MOS system depends in a self-consistent way on (a) the charge-density profile of mobile carriers which is induced via the gate voltage and the related surface electric field, and (b) the depletion field, which exists in the depletion layer of ionized acceptors and which can be varied by a substrate-bias voltage.[3] First calculations of energy eigenvalues and electron wave functions in this potential well have been carried out by Stern and Howard.[6] Within their effective-mass approximation the projection of the six volume-energy ellipsoids of Si onto the surface determines via the parallel masses m_x and m_y the parallel motion of the electrons. The z component of the effective-mass tensor governs the subband energies. In the triangular-well approximation the subband energies E_i are proportional to $m_z^{-1/3}$. Thus for Si(100) two subband systems exist. The energetically lower subband system (E_i) has a valley degeneracy $g_v=2$ with an isotropic parallel mass of $m_x=m_y=0.19m_0$ and a perpendicular mass $m_z=0.91m_0$. A second subband system, denoted by primes (E_i'), with $g_v=4$, $m_x=0.916m_0$, $m_y=0.19m_0$, and $m_z=0.19m_0$, is occupied for high charge densities.[17,18] For both subband systems the corresponding volume ellipsoids have their principal axis parallel or perpendicular to the surface.

The lowest subband system for Si(110) arises from the projection of four ellipsoids which are tilted with respect to the surface in the $[\bar{1}10]$ direction ($g_v=4$, $m_x=0.19m_0$, $m_y=0.55m_0$, and $m_z=0.31m_0$). The second subband system ($g_v=2$, $m_x=0.19m_0$, $m_y=0.916m_0$, and $m_z=0.19m_0$) is related to volume ellipsoids with their principal axes parallel to the surface. For Si(111) six equivalent valleys are occupied arising from the projection of all six volume ellipsoids, all tilted with respect to the surface ($g_v=6$, $m_x=0.19m_0$, $m_y=0.67m_0$, and $m_z=0.26m_0$).

More sophisticated calculations solve wave functions and energy eigenvalues self-consistently and include many-body corrections and the image potential (e.g., Refs. 19–23, 1, 4, 5 and 11). We like to draw attention to the image potential,[1]

$$V_I(z)=\frac{\epsilon_{sc}-\epsilon_{ox}}{\epsilon_{sc}+\epsilon_{ox}}\frac{e^2}{4\epsilon_{sc}},$$

which arises because of the difference in the dielectric functions of the semiconductor, ϵ_{sc}, and the insulator, ϵ_{ox}. Normally, the static values of ϵ are used. SiO_2 is an optically active material with the lowest-energy optical phonons at about 480 cm^{-1}. As pointed out in Ref. 1, the dispersion of ϵ_{ox} will lead to a renormalization of the subband energy if the polaron radius is comparable with the width of the electron wave functions, which is the case here. However, so far there exists no quantitative treatment of this effect. In our experiment this effect will be even more important since we will face the situation where intersubband resonance energies coincide with the optical-phonon frequencies of the SiO_2, so a resonance enhancement of this effect can be expected. We will discuss this point in more detail in Sec. IV F.

The resonance energy $\hbar\omega_{nm}$ that is measured in an intersubband experiment is not the separation $\hbar\omega_{nm}=E_m-E_n$ of the two subbands n and m, respectively, but is shifted due to two different mechanism. The first, the so-called depolarization effect or resonant screening effect, arises from the polarization of the electron gas in the finite potential well by the exciting field[24,25] and increases the resonance energy with respect to $\hbar\omega_{nm}$. The second effect arises from final-state interactions (exciton effect),[1,23] which, in general, lowers the resonance energy. The exciton effect is effective for both parallel and perpendicularly excited intersubband resonances. The depolarization shift is fully effective for perpendicular polarization, and it is canceled for parallel excitation on Si(111) and Si(110) if all valleys are occupied symmetrically in accordance with the effective-mass approximation.[5,7,8] In the following we denote exciton-shifted resonance transitions $n\rightarrow m$ by $\bar{E}_{nm}=\hbar\bar{\omega}_{nm}$ and both depolarization- and exciton-shifted resonances by $\tilde{E}_{nm}=\hbar\tilde{\omega}_{nm}$. The effect of the depolarization shift is usually characterized by an effective plasma frequency ω_{*nm} which is defined by $\omega_{*nm}^2=\tilde{\omega}_{nm}^2-\bar{\omega}_{nm}^2$.

In the approximation of a two-level model where only interactions of the two directly involved subands is taken into account, the resonance energies can be written as

$$\tilde{E}_{0n}=\hbar\tilde{\omega}_{0n}=\hbar\omega_{0n}(1+\alpha_{0n}-\beta_{0n})^{1/2}$$

and

$$\bar{E}_{0n}=\hbar\bar{\omega}_{0n}=\hbar\omega_{0n}(1-\beta_{0n})^{1/2},$$

where α_{0n} and β_{0n} are positive parameters which characterize, respectively, the depolarization and exciton effect. In more accurate calculations the depolarization and exciton shift of a certain transition, and thus also the effective plasma frequency, depend via rather complicated integrals on the shape and overlap of all wave functions.[23,25]

There has been an extensive discussion in the literature on the value of the valley degeneracy g_v for Si(111) and Si(110), particularly since in some Shubnikov–de Hass experiments $g_v=2$ has been measured in contrast to the effective-mass approximation (see discussion, e.g., in Refs. 1, 7, and 8). Both depolarization and exciton effects depend on g_v.[11,23] As discussed in great detail in Ref. 8 and also was found in Ref. 10, we see in our present experiment no evidence for deviations of the valley degeneracy from what one would expect from the effective-mass approximation, so we will not discuss the question of the valley degeneracy any further.

B. Grating couplers

The grating-coupler arrangement is shown schematically in Fig. 1. The gate of the MOS capacitor consists of periodic metal stripes with high and low conductivity, respectively. The width of the high-conductivity stripes is

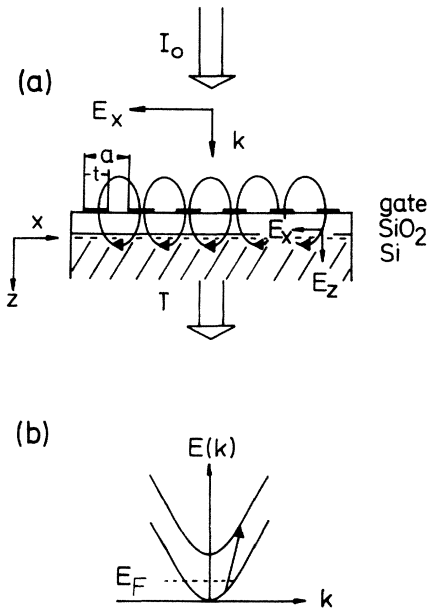

FIG. 1. Schematic MOS capacitor with a gate that consists of periodic metal stripes with high conductivity (in the regime t) and low conductivity (for the rest of the period a). For normally incident FIR radiation z components of the electric field, E_z, are induced, which make possible a perpendicular excitation of intersubband resonances. The grating-coupling-induced intersubband transitions are nonvertical, panel (b).

t, the periodicity is a. We assume that a is much smaller than the wavelengths λ of the normally incident FIR radiation. The x component of the FIR radiation, E_x, is zero in the highly conductive regime t. Thus the FIR field is spatially modulated in the near field of the grating and has there z components (E_z) that can induce perpendicular excitation of intersubband resonances (radiation polarized parallel to the grating stripes is reflected and cannot be observed in far-field transmission). The strength of the spatially modulated z component E_z can be calculated within the same approximation that has been used to calculate the spatially modulated x component (E_x) for the excitation of two-dimensional (2D) plasmons.[26,27] It depends on the ratio t/a and decreases approximately exponentially with the distance from the gate. We will not perform this calculation here, since the absorbed power depends, apart from the grating efficiency, on the intersubband transition matrix elements, which can only be calculated numerically.

An interesting feature of grating-coupler-induced intersubband resonances is pointed out in Refs. 13 and 14. Due to the spatial modulation of the exciting electric field, nonvertical intersubband resonances are induced (see Fig. 1). In particular, the quasimomenta of the electron wave functions for the excited (f) and ground (i) state differ by $\Delta k = k_f - k_i = 2\pi n/a$ ($n = 1,2,\ldots$). We will find in Sec. IV C that this has important consequences for the selection rules. In calculations of grating-coupler-induced intersubband resonances, it has also been found that broadening and shifts of the intersubband resonance line profile are expected if Δk approaches the Fermi wave vector k_F.[16] In our experiments here we always have $\Delta k \ll k_F$ and therefore do not describe this effect further.

In intersubband resonance experiments on InSb, perpendicularly excited intersubband resonances have been observed. The excitation is attributed to a random spatial variation of the incident field due to imperfections of the interface and of the insulating lacquer layer.[28]

III. SAMPLE PREPARATION AND EXPERIMENTAL TECHNIQUES

The experiments are performed on MOS capacitors with gates typically 5 mm in diameter. We use p-type Si substrates with substrate doping ranging from $N_A - N_D = (4-10)^{14}$ cm^{-3}. The grating structure shown in Fig. 1 is produced by first evaporating a thin NiCr gate of 5 nm thickness on the SiO_2 insulator. Periodic photoresist stripes are fabricated with two-beam laser interferometry on top of the NiCr film. These stripes serve as a mask for a shadowing process with 30 nm Al. In a lift-off technique the photoresist is removed and leaves periodic stripes of highly conducting Al. Grating periodicities for the samples used here range from 2000 to 500 nm, typical oxide thicknesses are $d_{ox} = 50$ nm.

The experimental techniques are similar to those of Ref. 10. The excitation of intersubband resonances is observed in the relative change of transmission,

$$\Delta T/T = [T(V_g) - T(V_t)]/T(V_t) \propto -\mathrm{Re}\sigma(\omega) ,$$

for FIR radiation transmitted normally through the sample at gate voltage V_g and at the conductivity threshold V_t, respectively. In the small-signal approximation, $-\Delta T/T$ is proportional to the real part of the dynamic 2D conductivity $\sigma(\omega)$.[1] The backside of the samples is wedged to avoid interference effects (wedge angle about 2°).

The experiments are performed in a rapid-scan Fourier-transform spectrometer. We measure alternatingly interferograms I of the transmitted radiation at gate voltage V_g and at threshold voltage V_t. The digitized interferograms $I(V_g)$ and $I(V_t)$ are co-added in different files and are Fourier-transformed at the end of the measurement. Thus very weak relative changes of the transmission can be measured with high signal-to-noise ratio and without problems from long-time drift of the experimental setup.

Spectra are measured in p-type samples at different depletion fields. Quasiaccumulation of electrons (depletion charge $N_{depl} = 0$) is induced by illuminating the substrate with band-gap radiation. The photoexcited carriers prevent the formation of a depletion layer. Inversion or substrate-bias conditions can be established in our MOS capacitors, which do not have drain and source contacts, in the following way. Synchronously with the mirror scans of the Fourier-transform spectrometer, the band-gap-illuminated MOS capacitor is charged at a certain voltage V_g. This voltage defines, via the capacitance, the charge density $N_s = \epsilon_{ox}(V_g - V_t)/ed_{ox}$. Before the sampling of the interferogram starts, the band-gap illumination is switched off and an additional substrate-bias volt-

age V_{SB} is added to V_g. Without illumination a depletion layer is formed. The delay ($t \approx 0.1$ s) between switching off the illumination and starting the sampling of the interferogram is chosen to be large enough to charge the depletion layer. The charge density N_{depl} of the depletion layer is calculated from the substrate doping and substrate-bias voltage with the formula[1]

$$N_{depl} = \left| \frac{2\epsilon_{sc}}{e} \phi_{depl}(N_A - N_D) \right|^{1/2},$$

where ϕ_{depl} is the sum of the conduction-band bending (1.1 eV) and the substrate-bias potential eV_{SB}. The substrate doping has been checked by C-V measurements and four-point resistivity measurements. We estimate the accuracy of determining N_{depl} to about 20%.

A more detailed description of the experimental setup and techniques is given in Ref. 29. All experiments are performed at 10 K with the spectral resolution of the spectrometer set to 2 cm^{-1}.

IV. EXPERIMENTAL RESULTS AND DISCUSSION

A. General aspects

In Fig. 2 we show original spectra measured on a Si(100) sample. The periodicity of the grating coupler is $a = 1.88$ μm, the oxide thickness is $d_{ox} = 45$ nm. The charge density N_s is 5.7×10^{-12} cm^{-2}. The spectra include different contributions to the high-frequency conductivity. The Drude-type intrasubband absorption background decreases continuously with increasing wave number. Resonances at low wave numbers are 2D plasmons of wave vector $q_n = 2\pi n/a$ ($n = 1,2,3$) which are excited via the spatially modulated x component E_x that is induced by the grating coupler. 2D plasmons have been studied extensively[26,27,30,31,13] and will not be treated here. At high wave numbers a sharp resonance is excited, which is smaller in amplitude than the plasmon excitation for $n = 1$ but can clearly be characterized in position and shape on the expanded scale. This resonance is the grating-coupler-induced $0 \rightarrow 1$ intersubband resonance. This type of excitation is the subject of this paper.

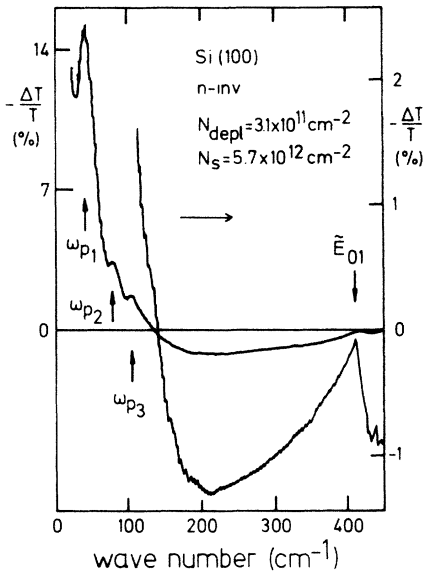

FIG. 2. Original spectra of the relative change in transmission $\Delta T/T$ versus wave numbers for electron inversion on a Si(100) sample with a grating coupler of periodicity $a = 1880$ nm. The charge density N_s and depletion charge N_{depl} are indicated. At high wave numbers the spectrum is also shown on an expanded scale (right-hand scale). Resonances ω_p at low wave numbers are 2D plasmon resonances. The resonance $\tilde{E}_{01}$ is the grating-coupler-induced intersubband resonance.

At a first glance it is surprising that in the wave number range above 100 cm^{-1} the signal $\Delta T/T$ is positive, which means that more light is transmitted through the sample with electrons in the channel. The electrons act in a way similar to an optical coating. In the linear approximation[26,27,30,31] electronic excitations absorb radiation and decrease the transmission. The complex optical behavior that is observed here is found to be typical for efficient grating couplers (see, e.g., Refs. 32 and 33). In particular, for the sample configuration used in Refs. 32 and 33 (an oxide-thickness-modulated MOS configuration) both polarization parallel and perpendicular to the grating stripes can be investigated, and it is found that only for FIR radiation polarized perpendicular to the grating stripes is the "positive" background signal observed. We will find in the following that the frequency dependence of the positive signal in $\Delta T/T$ is related to the frequency dependence of the dielectric function of SiO_2, and we will return to this point in Sec. IV F.

In spite of this complex behavior for the background, we can clearly extract from the experimental spectra the position and line shape of the intersubband resonance. The amplitudes of the grating-coupler-induced intersubband resonances vary for different samples depending on both the ratio t/a and the ratio d_{ox}/a.

B. Si(100)

In Fig. 3 we show measurements on a Si(100) sample similar to Fig. 2 ($a = 1.88$ μm, $d_{ox} = 45$ nm). The depletion charge is fixed ($N_{depl} = 2.2 \times 10^{11}$ cm^{-2}) and the surface electric field with corresponding charge density N_s is varied. At low N_s two resonances can be observed which can be identified as the $0 \rightarrow 1$ and the $0 \rightarrow 2$ transitions. Both resonances shift with increasing N_s to higher wave numbers.

In the wave-number regime 475–495 cm^{-1} there is a characteristic structure in all spectra. This is the frequency regime for optical phonons of SiO_2.[34,35] Our measurements show that there is a strong interaction of the optically active phonons in SiO_2 with the intersubband resonances. With increasing N_s the $0 \rightarrow 1$ transition is coupled to the optical-phonon frequency of SiO_2. This transition cannot be observed above the phonon frequency (at least up to frequencies of 700 cm^{-1} measured here); only the $0 \rightarrow 2$ transition is observed with decreased amplitudes above the phonon frequency. The background of the spectra jumps above the phonon frequency from negative values of $-\Delta T/T$ to nearly zero. This again suggests that the complex optical behavior discussed in Sec. IV A

is related to the oxide layer. We will discuss the interaction with the optical phonons of SiO_2 in more detail in Sec. IV F after we have shown results for the other surface orientations.

At the charge density $N_S \approx 7.5\times10^{12}$ cm^{-2} an additional resonance is observed which shifts with increasing N_s to higher wave numbers. This resonance is identified as a $0'\rightarrow1'$ transition in the second subband system ($g_v=4$) that exists on Si(100). The corresponding volume-energy ellipsoids are not tilted, and thus the grating coupler is needed to excite these resonances. For $N_{\text{depl}}=2\times10^{11}$ cm^{-2} it has been found[18] that the occupation of the E_0' subband starts at $N_{s0}=7.5\times10^{12}$ cm^{-2}, in agreement with our observation of the corresponding $0'\rightarrow1'$ transition.

We will discuss these $0'\rightarrow1'$ transitions in more detail below and the asymmetry of the $0\rightarrow1$ transition, which is observed in Fig. 3, in Sec. IV C.

The resonances shown in Fig. 3 are excited via the grating-coupler-induced z component (E_z) of the FIR field and thus represent depolarization- and exciton-shifted resonances $\tilde{E}_{nm}$. In Fig. 4 we have depicted ex-

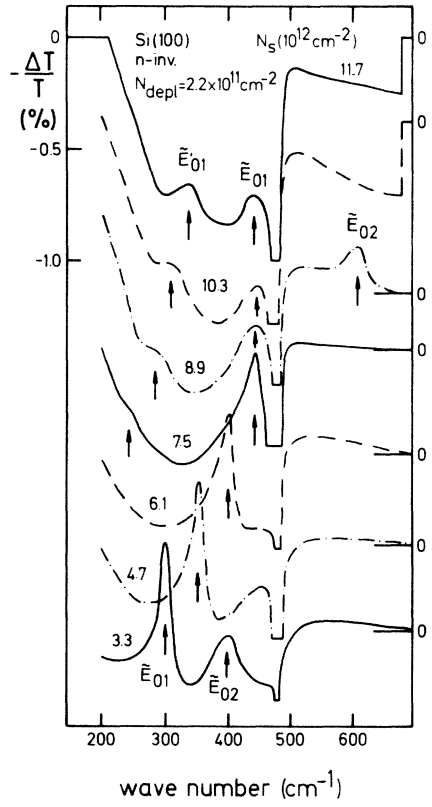

FIG. 3. Grating-coupler-induced intersubband resonances for Si(100) at different charge densities N_s. (Note the offset of the spectra for different N_s.) $N_{\text{depl}}=2.2\times10^{11}$ cm^{-2} is fixed. Resonances $\tilde{E}_{01}$ and $\tilde{E}_{02}$ in the lower subband system and $\tilde{E}'_{01}$ in the second subband system are observed. In the regime of the optical-phonon frequency of SiO_2 (about 480 cm^{-1}), a resonant structure is measured, which is not fully shown here for clarity. This structure will be discussed in Sec. IV F and in the caption of Fig. 17.

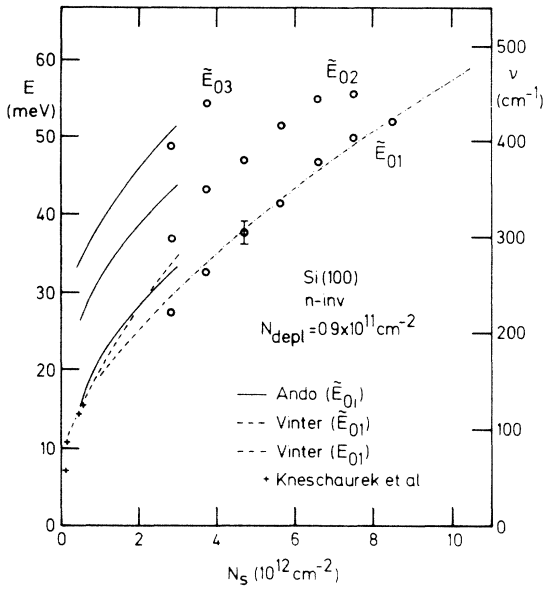

FIG. 4. Experimental intersubband resonance energies for Si(100) at $N_{\text{depl}}=0.9\times10^{11}$ cm^{-2}. The resonance energies are compared with calculated intersubband resonance positions $\tilde{E}_{0i}$ from Ando (Ref. 23) and Vinter (Ref. 22), with the subband separation E_{01} according to Vinter (Ref. 22) and with experimental data at low densities from Ref. 3. Data in Refs. 3, 22, and 23 are for $N_{\text{depl}}=1\times10^{11}$ cm^{-2}.

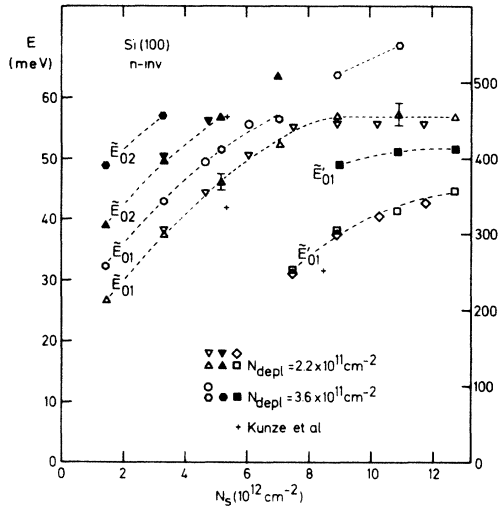

FIG. 5. Experimental intersubband resonance energies for Si(100) at different N_{depl}. Dashed lines are guides for the eye. The experimental resonance position from samples with different grating-coupler efficiency differ slightly near the SiO_2 phonon frequency of 480 cm^{-1}, and are identical within the experimental accuracy below 400 cm^{-1}. (∇,$\blacktriangledown$, $\Diamond$, $\circ$, sample 1; other symbols, sample 2. Sample 1 is also shown in Fig. 3, sample 2 in Fig. 4.) " + " denotes experimental subband separations from tunneling experiments (Ref. 38).

perimental resonance positions for inversion conditions ($N_{\text{depl}}=0.9\times10^{11}$ cm^{-2}). Three transitions, $\tilde{E}_{01}$, $\tilde{E}_{02}$, and $\tilde{E}_{03}$, are present. For inversion we are not able to observe intersubband resonances above the phonon frequency of SiO_2 (spectra are measured up to 700 cm^{-1}). Our resonance positions extrapolate well to experimental results which have been measured so far only at low densities (e.g., Ref. 3). Theoretical intersubband resonance energies, including depolarization and exciton shifts, are available up to densities of $N_s=3.0\times10^{12}$ cm^{-2}.[22,23] The resonance energies calculated there are slightly higher in energy than those found in our experiment. For the whole charge density regime covered in our experiment, only the subband separation E_{01}, without depolarization and exciton shift, has been calculated so far.[22] The data nearly coincide with our resonance energies $\tilde{E}_{01}$. This shows that subband calculations explain the general trend of the N_s dependence very well, but slight improvements of the theory are necessary to reproduce the experimental resonance positions, including depolarization and exciton shifts, correctly.

In Fig. 5 we have summarized experimental resonance positions for $N_{\text{depl}}=2.2\times10^{11}$ and 3.6×10^{11} cm^{-2}, respectively. The resonance energies shift with increasing depletion field to higher energies. There are no theoretical data available for these depletion charges. Also included are resonance positions in the primed subband system, which can be observed for $N_{\text{depl}}=2.2\times10^{11}$ cm^{-2} starting at $N_{s0}\approx7.5\times10^{12}$ cm^{-2} and for $N_{\text{depl}}=3.6\times10^{11}$ cm^{-2} at $N_{s0}\approx9\times10^{12}$ cm^{-2}. These N_{s0} values are in good agreement with data that have been found for the substrate-bias dependence of the second subband occupation (7.8×10^{12} and 8.6×10^{12} cm^{-2}, respectively) in Ref. 18.

Intersubband resonances in the primed subband system have been observed so far only at low densities where the E_0' subband has been occupied due to an increased temperature[36] or due to uniaxial stress.[37] Interestingly, we find that in contrast to the low-density, high-temperature results of Ref. 36 ($N_s=1.4\times10^{11}$ cm^{-2}, $T=28$ K) for our experiments at high $N_s>7\times10^{12}$ cm^{-2}, the $\tilde{E}_{01}'$ transition energy is smaller than the $\tilde{E}_{01}$ transition energy. This can be explained in the following way. At a fixed depletion field the energy E_0 of the lowest subband, measured with respect to the Fermi energy, decreases significantly with increasing charge density N_s. The energies of the higher subbands E_1, E_0', E_1', etc. are not so strongly effected by a variation of N_s, due to the screening of the electrons in the E_0 subband. Thus the $E_{01}=E_1-E_0$ transition energy increases strongly with N_s (due to E_0), where as E_{01}' increases only slowly with N_s. Thus E_{01} can be smaller at low N_s and larger at high N_s if compared with the slowly varying E_{01}'. This explanation is confirmed by measurements of the subband energies E_i and E_i' with tunneling spectroscopy.[38]

In Fig. 5 we also compare our experimental data with subband separations that have been found experimentally from tunneling spectroscopy on MOS samples with thin tunneling oxides at the same depletion charges.[38] Both the $0\rightarrow1$ and $0'\rightarrow1'$ separations of Ref. 38 are smaller in energy, which can be well explained by the additional depolarization shift of the intersubband resonance data. The depolarization shift for the $0\rightarrow2$ transition is smaller than for the $0\rightarrow1$, so the $\tilde{E}_{02}$ resonance energy is nearly the subband separation.[23] Here we find excellent agreement between intersubband resonance energy and subband separation from tunneling experiments.[38]

C. The line shape of resonances for Si(100)

The $\tilde{E}_{01}$ resonances observed in our spectra have a pronounced asymmetric profile. We find that on samples with different grating-coupler efficiency the peak position of the resonance is the same, but that with increasing grating-coupler efficiency an additional contribution on the low-energy slope of the resonance appears. Figure 6 shows measurements where this effect is very pronounced. The $\tilde{E}_{02}$ resonance, on the other hand, is rather symmetric. This leads us to the conclusion that the asymmetry of the $\tilde{E}_{01}$ transition is not caused by a deformation of the resonance profile that might be caused by the same mechanism that produces the positive background.

We believe that the shape of the resonance arises from intersubband transitions which are superimposed on the low-energy shoulder of the main resonance and which are not shifted due to a depolarization. Parallel excitation is strictly forbidden on samples without a grating coupler. Here the grating coupler induces spatially modulated x components of the FIR field. These spatially modulated x components induce nonvertical transitions $\Delta k=2\pi n/a$, so the selection rules for $\Delta k=0$ parallel excitation are no longer valid, and parallel excitation is possible. In Refs. 15 and 16 it has been calculated that for conditions simi-

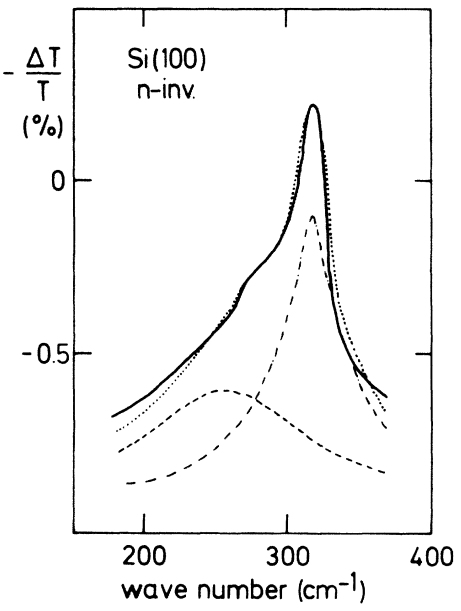

FIG. 6. Grating-coupler-induced intersubband resonance profile for Si(100), $N_s=2.9\times10^{12}$ cm^{-2}, $N_{\text{depl}}=3.6\times10^{11}$ cm^{-2}. The asymmetric profile is approximated by the superposition of two Lorentzian profiles. The lower resonance is attributed to possible intersubband transitions which are not affected by the depolarization shift.

lar to ours the nonvertical parallel excitation is smaller—by a factor of 10^5—than perpendicular excitation. In Fig. 6 we have superimposed two Loretnzian profiles to fit experimental resonance profile. We find that, if there is one low-energy resonance $\bar{E}_{01}$, it has a considerable amplitude of at least 10% of the depolarization-shifted amplitude $\tilde{E}_{01}$.

We suggest for the unexpected excitation of the $\bar{E}_{01}$ resonance the following explanation: The grating coupler induces electromagnetic waves with both wave vectors $+k_x$ and $-k_x$. Both waves have a fixed phase correlation and produce standing-wave-type electric field distribution, as shown for a fixed moment in time in Fig. 1. It is possible that this standing-wave-type electric field decreases the macroscopic polarization that is responsible for the depolarization shift. The exact excitation mechanism can only be explained by a rigorous grating-coupler theory.

The resonance profile for the $\tilde{E}_{02}$ transition (e.g., Fig. 3) is much more symmetrical than for the $\tilde{E}_{01}$ resonance. This is consistent with our explanation since the depolarization shift is much smaller for the E_{02} transition than for the E_{01} transition [see Ref. 23 and our experimental observations for Si(111) in Sec. IV D]. Thus, if there is a resonance $\bar{E}_{02}$, it cannot be resolved from $\tilde{E}_{02}$.

In Fig. 7 we have plotted $\tilde{E}_{01}$ and the resonance positions that we have attributed to $\bar{E}_{01}$. Within the relatively low accuracy of determining the position of the resonance $\bar{E}_{01}$, we can extract, from the differences of

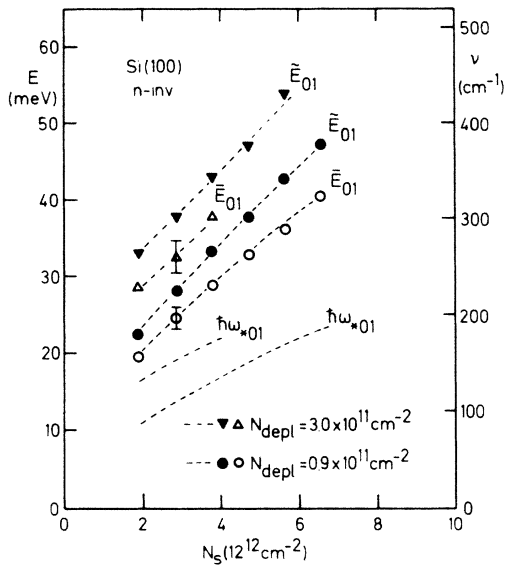

FIG. 7. Experimental resonance positions for Si(100) at different N_{depl}. $\tilde{E}_{01}$ is the depolarization-shifted intersubband resonance. $\bar{E}_{01}$ is the resonance position that is attributed to transitions which are not affected by depolarization and which are derived from fits similar to those shown in Fig. 6. The experimental data are connected by dashed lines for clarity. $\hbar\omega_{*01}$ is the effective plasma frequency that causes the depolarization shift. It is extracted from our experimental values of $\tilde{E}_{01}$ and $\bar{E}_{01}$.

depolarization-shifted resonances and the unshifted resonances,

$$\tilde{\omega}_{01}^2-\bar{\omega}_{01}^2=\omega_{*01}^2 ,$$

an effective plasma frequency, which gives, e.g., for $N_s=3\times10^{12}$ cm^{-2} and $N_{depl}=0.9\times10^{11}$ cm^{-2}, $\omega_{*01}=110$ cm^{-1}. This is comparable to effective plasma frequencies that we will find for Si(111) and Si(110) in Sec. IV. Calculations in Ref. 23 give, for $N_{depl}=1\times10^{11}$ cm^{-2} on Si(100), $\omega_{*01}=150$ cm^{-1}.

In Ref. 16 it has been calculated that there is a drastic change in the intersubband resonance line profile of nonvertical transitions if Δk is comparable or larger than $k_{F,01}=(2m_t\omega_{01}/\hbar)^{1/2}$ ($m_t=0.19m_0$ is the transverse mass). For our grating couplers $\Delta k=2\pi/a$ is less than 10% of $k_{F,10}$; thus these effects cannot be observed in our experiment, as has been calculated explicitly in Fig. 13 of Ref. 16.

We like to note that we have also tried to observe directly parallel excited intersubband resonances on Si(100) samples with continuous semitransparent gates without a grating coupler. Within our experimental sensitivity ($\Delta T/T<0.1\%$) we cannot find any evidence for the intersubband resonance excitation. This means that the interface and the oxides have very small irregularities which could, in principle, induce intersubband resonances as observed on InSb samples in Ref. 28. One aspect of these investigations was also to search for evidence of nonparabolicity for the inversion electron subband structure of Si.[39] As a possible explanation for an enhancement of the plasmon mass, which is observed for Si(100) at large charge densities N_s, an enhanced nonparabolicity of the 2D band structure has been discussed.[13,40] In systems with a nonparabolic band structure, direct parallel excitation of intersubband resonances is possible (see discussions in Refs. 1, 15, 16, and 28). However, the excitation of intersubband resonances via nonparabolicity is very weak, and thus the failure of observing intersubband resonances in parallel excitation without a grating coupler on Si(100) is not a very sensitive test, whether there is nonparabolicity or not.

D. Si(111)

The surface band structure of Si(111) arises from the projection of all six volume ellipsoids leading to a sixfold valley degeneracy. The ellipsoids are tilted with respect to the surface, and thus parallel excitation of intersubband resonances is possible and has been investigated in detail.[7,9,10] Perpendicular excitation has been studied at low densities in Refs. 7 and 9.

In Fig. 8 we show grating-coupler-induced intersubband resonance excitation on a Si(111) sample. The periodicity of the grating coupler is $a=750$ nm, the oxide thickness is $d_{ox}=45$ nm. In Fig. 8(a) experiments for $N_s=3.3\times10^{12}$ cm^{-2} and different depletion fields are depicted. For quasiaccumulation ($N_{depl}=0$) one asymmetric resonance is observed, which is very similar in shape to parallel excited intersubband resonances on samples without grating couplers[10] and which can be identified as $\bar{E}_{01}$, transitions unaffected by depolarization. In

the very shallow well of the accumulation potential, E_2 and higher subbands are smeared out and transitions to these subbands give rise to the continuous asymmetric line shape.[23]

For inversion ($N_{\text{depl}}=0.7\times10^{11}$ cm^{-2}) several resonances are observed in the spectra which are identified in the following as directly excited, $\bar{E}_{01}$, $\bar{E}_{02}$, and $\bar{E}_{03}$, transitions and grating-coupler-induced, depolarization-shifted, $\tilde{E}_{01}$, $\tilde{E}_{02}$, and $\tilde{E}_{03}$, resonances. This is the first time that the difference in frequency for the $\bar{E}_{02}$ and $\tilde{E}_{02}$ transitions is observed. It is significantly smaller than for the $0\rightarrow1$ transition, as has been calculated, e.g., in Ref. 23. We will discuss details of the depolarization shifts below. With increasing depletion charges the resonance energies shift to higher energies. This is caused by the larger subband separation in the steeper potential well for increasing depletion fields.

In Fig. 8(b) we have depicted grating-coupler-induced intersubband resonance spectra at different N_{depl} for a larger value of $N_s=7.7\times10^{12}$ cm^{-2}. In Fig. 9 we show for the fixed depletion charge $N_{\text{depl}}=2.9\times10^{11}$ cm^{-2} spectra at different charge densities N_s. The resonances shift with increasing N_s to higher energies. In Figs. 8 and 9 we notie an interaction of the intersubband resonances with the optical phonons in SiO_2 at frequencies around 480 cm^{-1}. The directly parallel excited resonances $\bar{E}_{01}$ and $\bar{E}_{02}$ are less affected, whereas the perpendicularly excited resonances are strongly decreased in amplitude above the phonon frequency. We will discuss this behavior in more detail in Sec. IV F.

For the excitation strengths of grating-coupler-induced intersubband resonances, we make characteristic observations.

(a) Using similar grating couplers the excitation strength is significantly stronger on Si(111) and Si(110) than on Si(100). The grating-coupler efficiency is characterized by the ratios t/a (see Fig. 1) and d_{ox}/a. For example, a grating coupler with $a=750$ nm and $d_{\text{ox}}=45$ nm induces, at Si(111), intersubband resonances of amplitudes shown in Figs. 8 and 9. For Si(100), with a grating coupler of the same geometry, very slight excitation of intersubband resonances is observed. Grating couplers with larger periodicities, $a=2$ μm, with corresponding smaller values of d_{ox}/a, are needed to excite intersubband resonances with amplitudes that are comparable to Si(111).

(b) For Si(111) in Fig. 8 we observe that the resonance amplitudes increase with increasing N_{depl}. This can be explained by a better overlap of the final and initial wave functions in the steeper potential well for larger depletion fields, which results in an increase of the oscillator strengths. We notice further that the amplitudes of the grating-coupler-induced and depolarization-shifted resonances $\tilde{E}_{01}$ increase with increasing N_{depl} significantly stronger than the parallel excited amplitudes. (For accumulation, e.g., $N_{\text{depl}}=0$, no perpendicularly excited resonance can be observed.) It seems that this effect is even more pronounced for higher transitions. For example, for $N_{\text{depl}}=0.7\times10^{11}$ cm^{-2} in Fig. 8(a) the $\tilde{E}_{01}$ resonance amplitude is smaller than the $\bar{E}_{01}$ amplitude, whereas it is the opposite for the $\tilde{E}_{02}$ and $\bar{E}_{02}$ resonance amplitudes. This indicates that there is a characteristic difference, for,

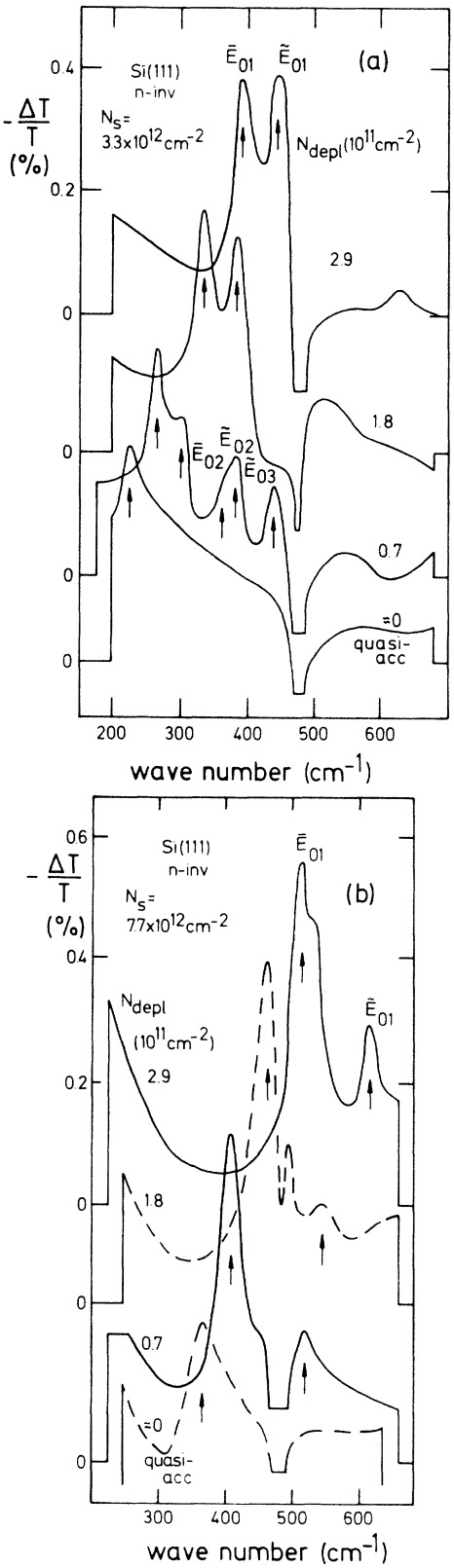

FIG. 8. Excitation of intersubband resonances on a Si(111) sample with a grating coupler for different N_{depl} and (a) $N_s=3.3\times10^{12}$ cm^{-2} and (b) $N_s=7.7\times10^{12}$ cm^{-2}, respectively. Directly parallel excited $\bar{E}_{0i}$ resonances and grating-coupler-induced depolarization-shifted $\tilde{E}_{0i}$ resonances are present. The structure at the phonon resonance near 480 cm^{-1} is not fully shown (see Fig. 17).

on one hand, the parallel oscillator strength, and, on the other hand, the perpendicular oscillator strength, in their dependence on N_{depl} and N_s, on the subband index, and also on the surface orientation.

In Fig. 10 we discuss experimental resonance frequencies for accumulation ($N_{depl}=0$) and inversion ($N_{depl}=0.7\times10^{11}$ cm^{-2}). The parallel excited intersubband resonance positions agree excellently with experimental results from Ref. 10 and, up to $N_s=6\times10^{12}$ cm^{-2}, with the accumulation data from Ref. 9 which have been measured without a grating coupler. At higher densities, the data of Ref. 9 are lower in energy. We have carefully checked by varying the intensity of the band-gap illumination that real accumulation conditions are established in our measurements. Perhaps the difference arises from the difference in the experimental technique, an N_s sweep in Ref. 9, and a frequency sweep here. If we extrapolated our resonance positions to N_{depl} and N_s used in Ref. 7, we find reasonable agreement with low-density data in Ref. 7 (sample 4, chip 1, Fig. 10 of Ref. 7).

As discussed above and shown in Fig. 8, we cannot observe the depolarization-shifted resonance for $N_{depl}=0$. For inversion in Fig. 10, the depolarization shift for the $0\rightarrow1$ transition is well pronounced. It is significantly smaller for the $0\rightarrow2$ transition and cannot be resolved for $0\rightarrow3$.

Theoretical data for Si(111) are available for accumulation at low densities[23] and are about 30 cm^{-1} above our

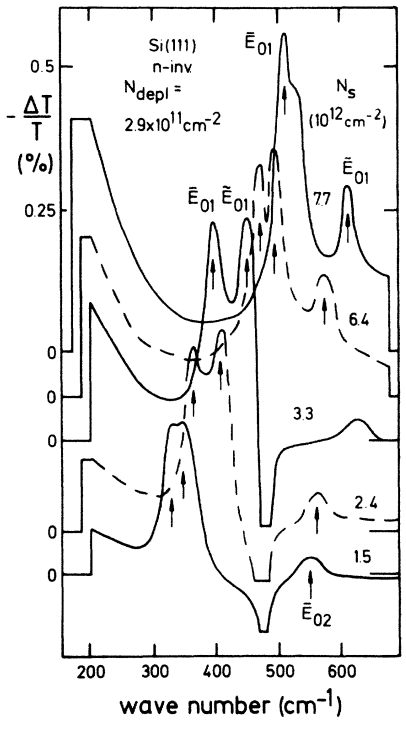

FIG. 9. Excitation of intersubband resonances on a Si(111) sample with a grating coupler for different N_s and fixed $N_{depl}=2.9\times10^{11}$ cm^{-2}. For further comments, see caption of Fig. 8.

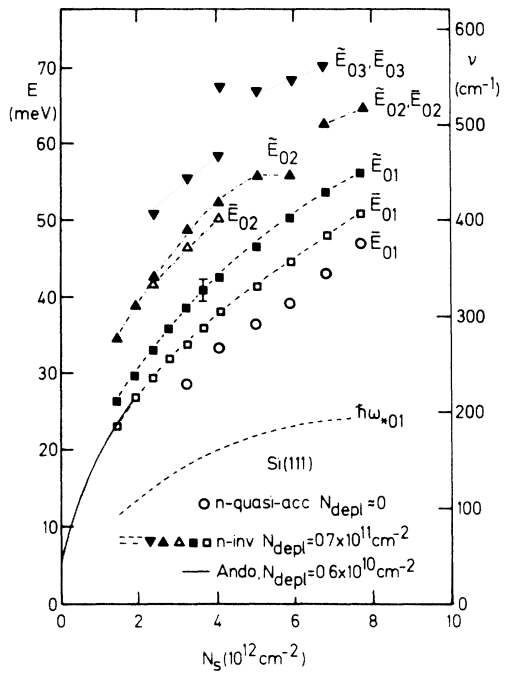

FIG. 10. Experimental intersubband resonance positions for electron accumulation and electron inversion on Si(111). Experimental data are connected by dashed lines for clarity. Theoretical $\bar{E}_{01}$ resonance energies from Ando (Ref. 23) for $N_{depl}=0.6\times10^{10}$ cm^{-2} are shown. For inversion the effective plasma frequency $\hbar\omega_{*01}$ is extracted from the experimental values of $\tilde{E}_{01}$ and $\bar{E}_{01}$. Above 480 cm^{-1}—the SiO_2 phonon frequency—we cannot decide unambiguously whether the resonances are $\bar{E}_{02}$ or $\tilde{E}_{02}$ transitions.

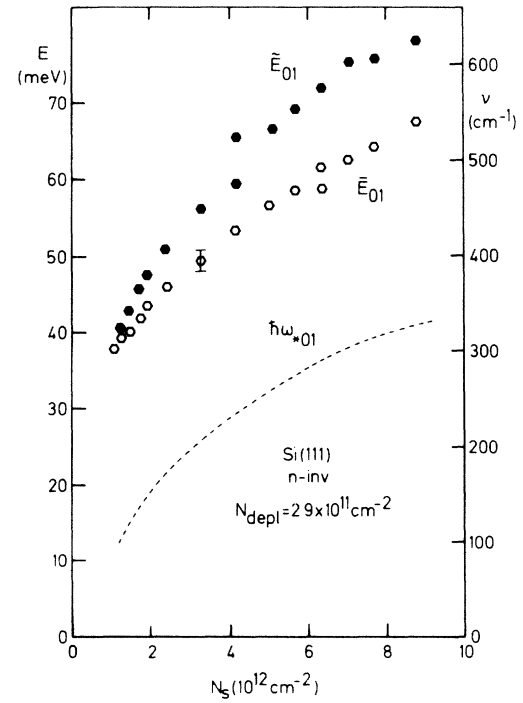

FIG. 11. Experimental intersubband resonance positions for $N_{depl}=2.9\times10^{11}$ cm^{-2} on Si(111). For further comments, see Fig. 10.

experimental resonance positions (theoretical data from Ref. 5 are much too high in energy; this is caused, as is stated in this reference, by the approximate variational method used there).

In Fig. 11 we have plotted experimental resonance positions from substrate-bias experiments ($N_{\rm depl}=2.9\times10^{11}$ cm^{-2}). Theoretical data are so far not available. For all spectra the interaction with optical phonons in SiO_2 is present.

In Fig. 12 we have extracted from our experimental data the dependence of the resonance position on $N_{\rm depl}$ at two fixed charge densities. Both the transition energy and the depolarization shift increase with $N_{\rm depl}$.

The observation of both the parallel excited and depolarization-shifted perpendicularly excited intersubband resonances in our spectra offers the unique possibility of characterizing the depolarization shift in detail. From the difference $\tilde{\omega}_{nm}^2-\bar{\omega}_{nm}^2=\omega_{*nm}^2$, we can evaluate the effective plasma frequency. It is extracted from our data and included in Figs. 10–12. For example, for inversion in Fig. 10, ω_{*01} is 105 cm^{-1} at $N_s=1.5\times10^{12}$ cm^{-2} and increases to 195 cm^{-1} at $N_s=8\times10^{12}$ cm^{-2}. The effective plasma frequency for the 0→2 transition is, as expected from theory,[23] smaller (e.g., at $N_s=4\times10^{12}$ cm^{-2}, it is $\omega_{*02}=110$ cm^{-1}, whereas $\omega_{*01}=160$ cm^{-1}). The increase of the effective plasma frequency with $N_{\rm depl}$ is shown in Fig. 12. There are so far no calculations of depolarization shifts and exciton shifts available for the charge density and depletion charge regime covered here.

Whereas for Si(100) the exciton effect is important and, at low densities, nearly cancels the depolarization shift, it is of less importance for Si(111) and Si(110) due to the smaller m_z. If we use the two-level approximation (see Sec. II A) and if we neglect β_{01} at large N_s, we can approximately extract the depolarization-shift coefficient α_{01}. For Si(111) we find, at $N_s=8.0\times10^{12}$ cm^{-2}, $\alpha_{01}=0.22$ for $N_{\rm depl}=1.0\times10^{11}$ cm^{-2}, and $\alpha_{02}=0.36$ for $N_{\rm depl}=3.0\times10^{11}$ cm^{-2}.

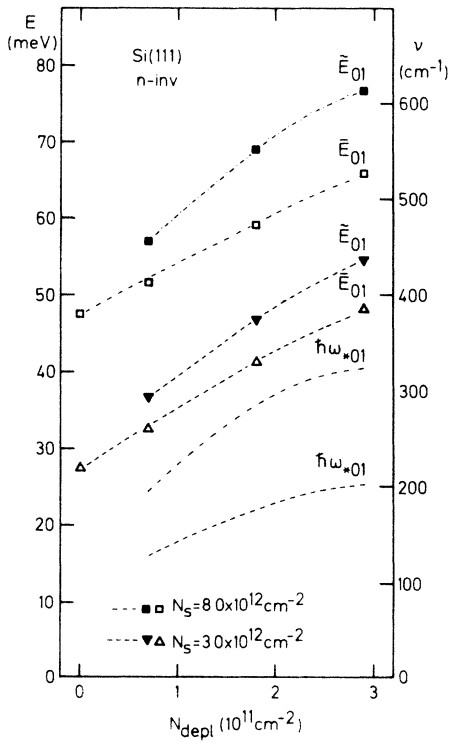

FIG. 12. Dependence of the experimental intersubband resonance energies and of the extracted effective plasma frequencies on the depletion charge $N_{\rm depl}$ for Si(111) at two different N_s.

E. Si(110)

The lowest subband system for Si(110) arises from the projection of four ellipsoids which are tilted with respect to the surface in the [$\bar{1}$10] direction ($g_v=4$, $m_x=0.19m_0$, $m_y=0.53m_0$, and $m_z=0.315m_0$). This surface is anisotropic. Direct parallel excitation of intersubband resonances is possible only with electric field components in the [$\bar{1}$10] direction.[8,10] The second subband system ($g_v=2$, $m_x=0.916m_0$, and $m_y=m_z=0.19m_0$) can only be excited via E_z.

Many properties of Si(110) are qualitatively similar to Si(100) and Si(111). We will treat this surface briefly and concentrate here on (a) the anisotropy and (b) the question of the occupation of the second subband system E'.

In Fig. 13 we compare measurements on two Si(110) samples with different polarization directions of the grat-

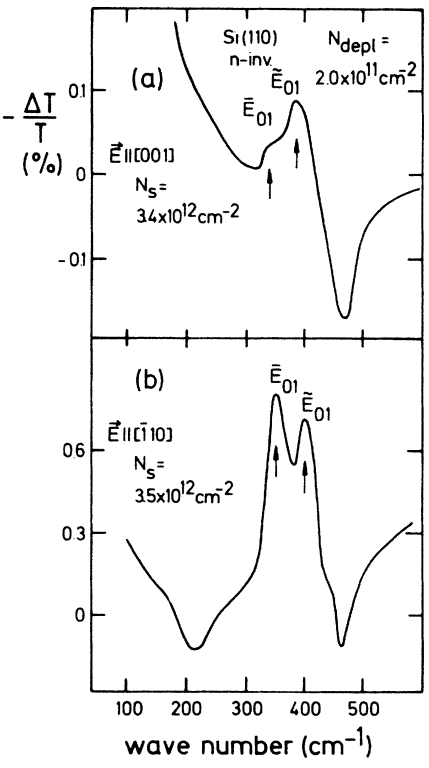

FIG. 13. Intersubband resonance excitation on Si(110) samples with grating couplers that polarize the exciting electric field **E** (a) parallel to the [001] direction and (b) parallel to the [$\bar{1}$10] direction, respectively. For **E**||[001] only a weak excitation of $\bar{E}_{01}$ is observed, whereas for **E**||[$\bar{1}$10], the tilt direction of the ellipsoids, both $\bar{E}_{01}$ and $\tilde{E}_{01}$ transitions are excited with significant strength. Note the difference in the scales for (a) and (b).

ing. The grating couplers have periodicities $a \approx 500$ nm and an oxide thickness $d_{ox} = 45$ nm. For a grating that polarized the FIR radiation in the [001] direction, we observe a resonance $\tilde{E}_{01}$. This resonance is excited via the grating coupler (it cannot be observed without a grating coupler in parallel excitation[10]) and thus represents the depolarization-shifted resonance.

The line shape of the intersubband resonances for the [001] direction of Si(110) is asymmetric. So, as has been discussed for Si(100) in Sec. IV C, parallel excited transition $\bar{E}_{01}$ seem to be present at energies below $\tilde{E}_{01}$.

For the [$\bar{1}$10] direction in Fig. 13 both directly parallel excited and grating-coupler-induced perpendicularly excited resonances are observed. The dependence of the spectra on the depletion charge is shown for two charge densities in Fig. 14. The resonances shift with both N_{depl} and N_s to higher energies. Resonances for accumulation are broader than for parallel excitation on similar samples without a grating coupler.[10] Thus one can expect that the resonances for accumulation in Fig. 14 include both $\bar{E}_{01}$ and $\tilde{E}_{01}$ resonances, which cannot be resolved separately.

For the excitation strength and its dependence on N_s and N_{depl}, we find for the [$\bar{1}$10] direction similar results as for Si(111). For the [001] direction the excitation strength for comparable grating couplers is weaker than for the [$\bar{1}$10] direction [see scales in Fig. 13(a) and (b)] and for Si(111), but it is stronger than for Si(100).

In Fig. 14 we notice—at frequencies around 200 cm^{-1}—a resonant structure that is superimposed on the decreasing background. This structure is relatively weak and cannot be subtracted with high accuracy from the background of the spectra, but we shall point out that there are some arguments that this structure perhaps arises from $0' \rightarrow 1'$ resonances in the $g_v = 2$ subband system, which can only be excited via E_z. The position depends on N_{depl}, as expected from an intersubband resonance. It does not depend significantly on the surface electric field and on N_s. However, for Si(110) it is quite possible that the subband energy of the primed subband system is pinned near the unprimed system. The density of states for the primed system is lower than for the unprimed system, and more electrons are in the unprimed system. A variation in N_s mainly changes the lower part of the potential $V(z)$ for small z. Subband energies for the primed system depend on the potential $V(z)$ at large values of z. It can be influenced significantly only by the depletion field. The surface electric field is predominantly screened by the electrons in the lower subband system.

From our experiments we conclude that the primed subband system is already occupied at relatively low densities. We cannot extract from our measurements an exact onset of the occupation, but resonances can be observed at least at $N_s > 1.0 \times 10^{12}$ cm^{-2}. Calculations of the Si(110) subband structure, including both subband systems, are rare and so far unclear concerning the second subband. According to Ref. 19 all electrons are in the lowest subband at $T = 0$ and $N_s < 10^{13}$ cm^{-2}. In Ref. 41 it is stated that occupation of the primed subband should occur below $N_s = 5 \times 10^{12}$ cm^{-2}. To our knowledge so far, occupation of the primed subband system has not been observed in Shubnikov–de Haas (SdH) measure-

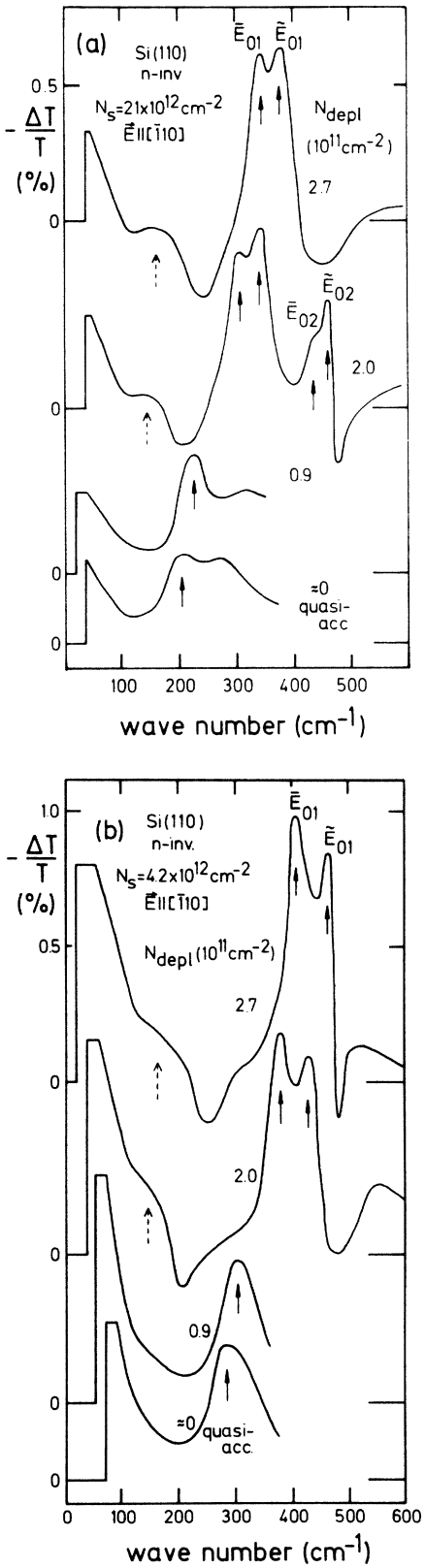

FIG. 14. Intersubband resonance excitation on a Si(110) sample with a grating coupler that polarized the exciting field **E** parallel to the [$\bar{1}$10] direction. Spectra for different N_{depl} are shown. N_s is 2.1×10^{12} cm^{-2} in (a) and 4.2×10^{12} cm^{-2} in (b). The weak structures denoted by dashed arrows are possibly transitions in the primed subband system E'.

ments.[42,43] However, if our interpretation of a strong pinning for the primed subband system, and thus nearly constant values for the density N_s' in the primed system is right, then occupation of E_0' cannot be detected in N_s-sweep SdH experiments.

Evidence for the occupation of the primed subband system also comes from plasmon resonance measurements.[40] There one finds that the plasmon mass in the $[\bar{1}10]$ direction is smaller and the plasmon mass in the [001] direction is larger than expected for the $g_v=4$ system. This is exactly the case if both subband systems are occupied, since the (reciprocal) plasmon mass in a multivalley system is the averaged reciprocal mass of all occupied valleys.[40]

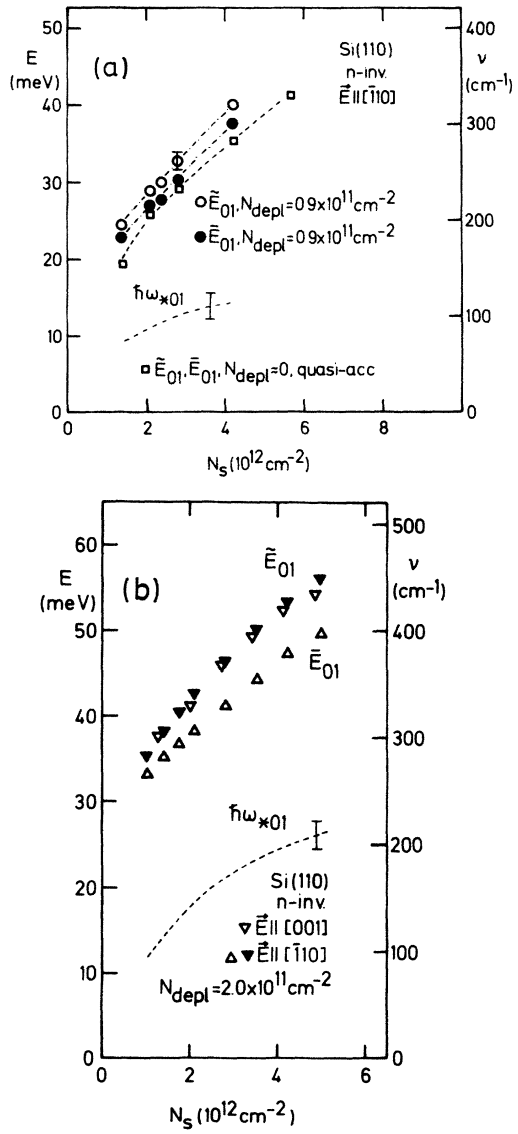

FIG. 15. Experimental intersubband resonance positions. (a) quasiaccumulation and inversion on Si(110) measured for $\mathbf{E}||[\bar{1}10]$; (b) substrate-bias conditions ($N_{depl}=2.0\times10^{12}$ cm^{-2}). Within the experimental accuracy there is no difference for the $\tilde{E}_{01}$ transition measured for $\mathbf{E}||[\bar{1}10]$ and $\mathbf{E}||[001]$, respectively. $\hbar\omega_{*01}$ is the effective plasma frequency extracted from the experimental resonance positions $\tilde{E}_{01}$ and $\bar{E}_{01}$.

As stated above, the structures that we attribute to the primed subband transitions are weak, and experiments with grating couplers of higher efficiency are necessary to confirm our explanation unambiguously. Also, it would be helpful to have self-consistent calculations for the complex subband structure of Si(110).

In Fig. 15 we have depicted experimental resonance positions for accumulation and inversion. The accumulation data, where we cannot separate $\bar{E}_{01}$ and $\tilde{E}_{01}$ transitions, are slightly higher than $\bar{E}_{01}$ data for parallel excited resonance positions (without a grating coupler) in Refs. 8 and 10. At low densities theoretical data are available[23,44] and are slightly higher than our experimental data. We like to note that, within the experimental accuracy, we cannot resolve a difference in the resonance positions for the $\tilde{E}_{01}$ resonances measured in the $[\bar{1}10]$ or in the [001] direction [Fig. 15(b)].

The depolarization shifts $\Delta\omega$ that we measure on Si(110) are similar to those from measurements on Si(111). For example, for $N_s=2.1\times10^{12}$ cm^{-2} and inversion ($N_{depl}=0.9\times10^{11}$ cm^{-2}), we find, for Si(111), $\Delta\omega=22$ cm^{-1}, and for Si(110), 18 cm^{-1} (Fig. 16). Experimental data from Ref. 8 on Si(110) give for accumulation much higher values ($\Delta\omega=58$ cm^{-1}), whereas experimental data for accumulation[9] on Si(111) are similar to ours (22 cm^{-1}). In Refs. 8 and 9 transmission line experiments at low densities and parallel excitation are compared. From the low-density data in Ref. 7 ($N_{depl}\approx1\times10^{11}$ cm^{-2}) on Si(110), we extrapolate a depolarization shift $\Delta\omega=26$ cm^{-1} for $N_s=2.0\times10^{12}$ cm^{-2}, which is comparable to our data ($\Delta\omega=18$ cm^{-1} for $N_{depl}=0.9\times10^{11}$ cm^{-2}). We like to note that in the arrangements of Refs. 7–9 the samples need a semitransparent gate to measure $\bar{E}_{01}$ and a highly conducting gate to determine $\tilde{E}_{01}$. Thus the depolarization shift is extracted from data measured in different spectra with slightly different sample geometry. In our measurements, $\bar{E}_{01}$ and $\tilde{E}_{01}$, and thus the depolarization shift, are measured simultaneously in one spectrum, and thus have the same sample geometry.

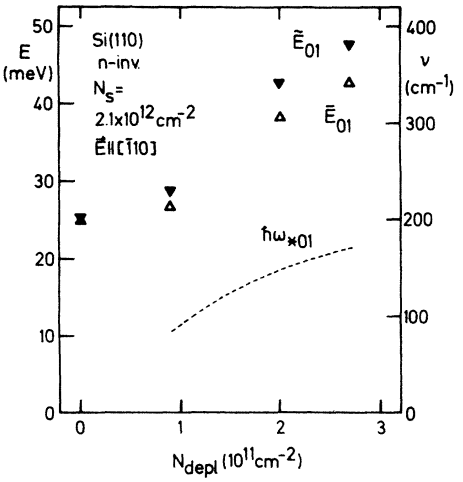

FIG. 16. Dependence of the experimental intersubband resonance positions and the extracted effective plasma frequency $\hbar\omega_{*01}$ on the depletion charge N_{depl} for Si(110).

F. Interaction of optical phonons in SiO_2 with intersubband resonances

In the experimental spectra shown above, we observe for the first time a strong interaction of the intersubband resonance with optical phonons in SiO_2. The TO and LO modes of SiO_2 are, according to Ref. 35, 455 and 494 cm^{-1}, respectively, but in amorphous SiO_2 the reststrahlen band is smeared out and data for the phonon frequencies, damping, and oscillator strength differ in the literature (e.g., Refs. 34 and 35). The peak position for the phonon effect in our experiments (e.g., Fig. 10) is 478 cm^{-1}.

There are two aspects of the interaction with phonons in SiO_2. The first, the polaron aspect, concerns the subband energies and intersubband resonances in a 2D system with an adjacent dispersive polar media. In Ref. 1 it was discussed that the dispersion of SiO_2 leads to a renormalization of the image potential and thus the subband energies, if the polaron radius $r_p=(\hbar/m_z\omega_s)^{1/2}$ (ω_s is the phonon frequency) is comparable with the thickness of the inversion layer. For Si(111), with $m_z=0.26m_0$, r_p is about 2 nm. Typical inversion layer thicknesses, e.g., at $N_s=5\times10^{12}$ cm^{-2}, are about 3 nm. Thus the renormalization is effective here.

As it has been stated in Ref. 1, there are no calculations of this polaron effect available so far. (In Ref. 21 the renormalization of the effective parallel mass due to the SiO_2 dispersion has been calculated.) For our dynamical intersubband resonance experiments this effect can be even more important, since one can well expect that, if the intersubband resonance approaches ω_s, a resonant interaction can occur, similar to what has been observed for resonant polaron effects on the cyclotron mass of 2D inversion electrons near the reststrahlen band of polar semiconductors (e.g., Ref. 45). Such resonant behavior can cause a pinning of the intersubband resonances at the phonon frequency.

The second aspect of phonon interactions in SiO_2 concerns the excitation process via the grating coupler with a dispersive dielectric material between grating and inversion layer. The dielectric function $\epsilon_{ox}(\omega)$ of the SiO_2 films shows, in the regime of the phonon frequencies, the well-known behavior of a phonon oscillator; in particular, $\epsilon_{ox}(\omega)$ approaches 0 at the LO frequency.

Let us denote the directly excited parallel x component, E_x, of the electric field that is induced by the incident FIR radiation in the plane of the inversion layer ($z=d_i$) as $E_{x0}=E_x(\omega, q=0, z=d_i)$ and the spatially modulated field component E_z that is induced by the grating coupler in the inversion layer by $E_{zq}=E_z(\omega, q=2\pi/a, z=d_i)$. We assume that the grating-coupler efficiency is such that both amplitudes E_{x0} and E_{zq} are about the same at $z=d_i$ for frequencies far below ω_{TO}, where $\epsilon_{ox}(\omega)$ has nearly the static value. One can then calculate from the Fresnel coefficients for our system in Fig. 1 that the grating-coupler-induced perpendicular fields E_{zq}, with large values of $q\gg\omega/c$, are more affected if $\epsilon(\omega)$ approaches zero ($\omega\rightarrow\omega_{LO}$) than the parallel field E_{x0} with wave vector $q=0$. Expressed in a different way, we can say that the SiO_2 layer represents a thin slab that can be polarized better with a perpendicular field than with a parallel field. For small ϵ_{ox} the ratio of the amplitudes E_{zq}/E_{x0} decreases approximately in proportion with $(\epsilon_{ox})^{1/2}$. This is one of the reasons why the grating-coupler-induced intersubband resonance is observed with less intensity above ω_{LO}, where $\epsilon_{ox}(\omega)$ is still smaller than below ω_{TO}, and why the parallel excited resonances, e.g., in Figs. 8(b) and 9, are less affected by the phonons in SiO_2.

In Fig. 17 we have plotted spectra for electron inversion in Si(100). Here we show fully the resonant positive signals in $\Delta T/T$ at frequencies of about 480 cm^{-1} that have been suppressed in the preceding figures for a clear representation of the intersubband resonances in their dependence on N_s or N_{depl}. The strength of this resonant signal increases with N_s. We explain this resonance in the following way. In a polar material a polariton-type excitation exists below ω_{LO}.[46] If there are no electrons in the channel ($V_g=V_t$), then the incident radiation is coupled via the grating coupler to these polaritons, giving rise to a resonant absorption in the spectra $T_0(\omega)$. With mobile electrons in the channel ($V_g>V_t$), the excitation of these polaritons and the absorption is suppressed. Thus more FIR radiation is transmitted through the sample and yields a positive value of $\Delta T/T$.

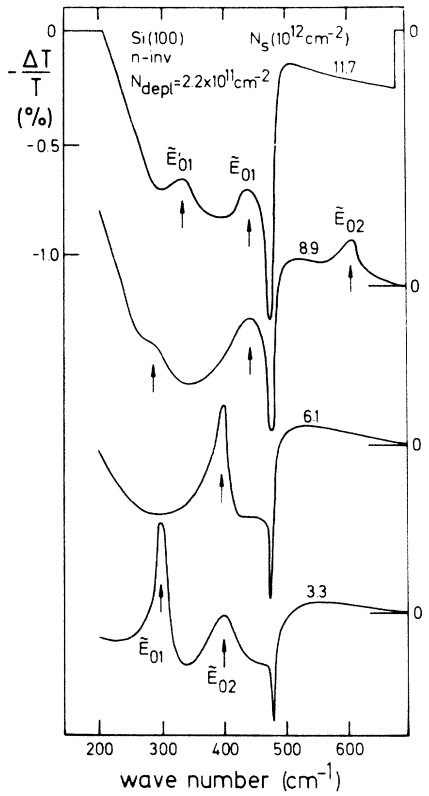

FIG. 17. Relative change of transmission for a Si(100) sample with a grating coupler. In addition to intersubband resonance excitations, a structure at the SiO_2 optical-phonon frequency (about 480 cm^{-1}) is observed. This structure indicates that for $N_s=0$ there is a resonant excitation of polaritons via the grating in the SiO_2 layer. With increasing N_s this excitation is suppressed, giving rise to a positive relative change of the transmission, $\Delta T/T$.

Polaritons are (resonant) electrodynamic excitations with wave vectors $q = 2\pi n/a > \omega/c$ and with fields that decay exponentially outside the oxide layer. Similarly, (nonresonant) evanescent electrodynamic waves are induced via the grating coupler also in the frequency range outside the polariton regime. The influence of a space-charge layer on these waves will affect indirectly and in a complex way the transmission of FIR radiation through the sample, in addition to the direct coupling (Drude absorption). Since the evanescent waves are concentrated to a large extent in the SiO_2 layer, the effect will be related to the frequency dependence of the dielectric function of the oxide as observed in the experiment (e.g., Fig. 17). This indirect grating-coupler-induced interaction can explain the "positive" background. The increase of transmission with electrons in the channel may be caused by a suppression of the evanescent waves, resulting in a decrease of absorption and reflection. A quantitative explanation, however, can only be given by a rigorous grating-coupling theory.

Thus the complex behavior of the intersubband resonance in the regime of the SiO_2 phonon frequencies arises from two effects: (a) the resonant renormalization of the intersubband resonance frequencies (polaron effects) near ω_s, and (b) the frequency- and q-dependent coupling efficiency of the grating, including polariton effects. For a quantitative explanation, both an intersubband resonance excitation theory including polaron effects and an exact, frequency- and q-dependent grating-coupler theory for the excitation are necessary. From the fact that the parallel excited resonances are only slightly affected by the phonons in SiO_2, one can conclude that the polaron effect is small. However, for perpendicular excitation the question is how a resonant polaron is defined in a system that is strongly coupled to polariton excitation. The situation in our experiment is similar to the observation of intersubband resonances in polar semiconductors.[47]

We would like to note there that for parallel excitation on samples without a grating coupler a resonant interaction with optical phonons in Si at frequencies around 520 cm^{-1} has been observed.[48] For hole space-charge layers this interaction is relatively strong and can be attributed to a deformation-type electron—optical-phonon interaction. For electron space-charge layers the interaction with optical phonons in Si is found to be very weak. Perhaps the fine structure of the intersubband resonance profile for the $\bar{E}_{01}$ resonance at $N_s = 7.7 \times 10^{12}$ cm^{-2} in Fig. 9 is caused by an interaction with optical phonons of Si.

V. CONCLUSIONS

Efficient grating couplers have been used to investigate the subband structure and intersubband resonance transitions in electron space-charge layers for the principle surfaces of Si.

For Si(100) perpendicularly excited intersubband resonances have been investigated up to charge densities of $N_s = 1.2 \times 10^{13}$ cm^{-2}. At high N_s, transitions in the primed subband system are observed. For Si(111) and for the $[\bar{1}10]$ direction of Si(110), both directly excited parallel resonances and perpendicularly excited depolarization-shifted resonances are observed, and the depolarization shift is studied in detail in its dependence on the surface electric and depletion fields and on the subband index. There is a characteristic dependence of the excitation strength of intersubband resonances on the surface orientation, on the polarization, on N_s, on N_{depl}, and on the subband index.

For Si(100) there is evidence of parallel excited resonances which are not affected by depolarization and which arise from grating-coupler-induced nonvertical transitions. On all surfaces there is a strong interaction of the intersubband resonances with optical phonons in SiO_2.

ACKNOWLEDGMENTS

We would like to thank J. P. Kotthaus for valuable discussions, and W. Beinvogl of Siemens, Munich, for supplying the Si wafers, and we would also like to acknowledge financial support of the "Stiftung Volkswagenwerk."

[1]For a recent review, see T. Ando, A. Fowler, and F. Stern, Rev. Mod. Phys. **54**, 437 (1982).
[2]J. F. Koch, Surf. Sci. **58**, 104 (1976).
[3]P. Kneschaurek, A. Kamgar, and J. F. Koch, Phys. Rev. B **14**, 1610 (1976).
[4]T. Ando, T. Eda, and M. Nakayama, Solid State Commun. **23**, 751 (1977).
[5]K. S. Yi and J. J. Quinn, Phys. Rev. B **27**, 2396 (1983).
[6]F. Stern and W. E. Howard, Phys. Rev. **163**, 816 (1967).
[7]T. Cole and B. D. McCombe, Phys. Rev. B **29**, 3180 (1984).
[8]Soe-Mie Nee, U. Claessen, and F. Koch, Phys. Rev. B **29**, 3449 (1984).
[9]F. Martelli, C. Mazuré, and F. Koch, Solid State Commun. **49**, 505 (1984).
[10]A. D. Wieck, E. Batke, D. Heitmann, and J. P. Kotthaus, Phys. Rev. B **30**, 4653 (1984).
[11]S. Das Sarma and B. Vinter, Phys. Rev. B **28**, 3639 (1983).
[12]B. D. McCombe, R. T. Holm, and D. E. Schafer, Solid State Commun. **32**, 603 (1979).
[13]D. Heitmann, J. P. Kotthaus, and E. G. Mohr, Solid State Commun. **44**, 715 (1982).
[14]E. Batke, D. Heitmann, and E. G. Mohr, Physica **117&118B**, 643 (1983).
[15]T. W. Nee, Phys. Rev. B **29**, 3225 (1984).
[16]T. W. Nee and F. Koch, Phys. Rev. B **29**, 3239 (1984).
[17]D. C. Tsui and G. Kaminsky, Phys. Rev. Lett. **35**, 1468 (1975).
[18]G. M. Gusev, Z. D. Kvon, and V. N. Ovsyuk, Solid State Commun. **49**, 899 (1984).
[19]F. Stern, Phys. Rev. B **5**, 4891 (1972).
[20]T. Ando, Phys. Rev. B **13**, 3468 (1976).
[21]B. Vinter, Phys. Rev. B **13**, 4447 (1976).
[22]B. Vinter, Phys. Rev. B **15**, 3947 (1977).
[23]T. Ando, Z. Phys. B **26**, 263 (1977).

[24]W. P. Chen, Y. J. Chen, and E. Burstein, Surf. Sci. **58**, 263 (1976).
[25]S. J. Allen, D. C. Tsui, and B. Vinter, Solid State Commun. **20**, 425 (1976).
[26]S. J. Allen, Jr., D. C. Tsui, and R. A. Logan, Phys. Rev. Lett. **38**, 980 (1977).
[27]T. N. Theis, J. P. Kotthaus, and P. J. Stiles, Solid State Commun. **24**, 273 (1977).
[28]K. Wiesinger, H. Reisinger, and F. Koch, Surf. Sci. **113**, 102 (1982).
[29]E. Batke and D. Heitmann, Infrared Phys. **24**, 189 (1984).
[30]D. C. Tsui, S. J. Allen, Jr., R. A. Logan, A. Kamgar, and S. N. Coppersmith, Surf. Sci. **73**, 419 (1978).
[31]T. N. Theis, Surf. Sci. **98**, 515 (1980).
[32]U. Mackens, D. Heitmann, L. Prager, J. P. Kotthaus, and W. Beinvogl, Phys. Rev. Lett. **53**, 1485 (1984).
[33]D. Heitmann, J. P. Kotthaus, U. Mackens, and W. Beinvogl, Superlattices Microstruct. **1**, 35 (1985).
[34]M. Miler, Czech. J. Phys. B **18**, 354 (1968).
[35]F. L. Galeener and G. Lucovsky, Phys. Rev. Lett. **37**, 1474 (1976).
[36]P. Kneschaurek and J. F. Koch, Phys. Rev. B **16**, 1590 (1977).
[37]S. Oelting, D. Heitmann, and J. P. Kotthaus, Phys. Rev. Lett. (to be published).
[38]U. Kunze and G. Lautz, Surf. Sci. **113**, 55 (1982); U. Kunze, Phys. Rev. B **32**, 5328 (1985).
[39]L. M. Falicov, Solid State Commun. **18**, 669 (1976).
[40]E. Batke and D. Heitmann, Solid State Commun. **47**, 819 (1983).
[41]F. Stern, cited in Ref. 42.
[42]T. Neubauer, K. von Klitzing, G. Landwehr, and G. Dorda, Solid State Commun. **17**, 295 (1975).
[43]K. C. Woo and P. J. Stiles, Phys. Rev. B **28**, 7101 (1983).
[44]B. Vinter, cited in Ref. 8.
[45]M. Horst, U. Merkt, and J. P. Kotthaus, Phys. Rev. Lett. **50**, 754 (1983).
[46]*Electromagnetic Surface Modes,* edited by A. D. Broadman (Wiley, Chichester, 1982).
[47]J. Scholz, F. Koch, H. Maier, and J. Ziegler, Solid State Commun. **45**, 39 (1983).
[48]D. Heitmann, E. Batke, and A. D. Wieck, Phys. Rev. B **31**, 6865 (1985).